Materials Transactions, Vol. 57, No. 7 (2016) pp. 1138 to 1146

Effects of Heat Exposure Time and Temperature on the Delamination Behavior of Air Plasma-Sprayed Thermal Barrier Coatings under Shear Loading

Makoto Hasegawa[*1], Tsuyoshi Endo[*2] and Hiroshi Fukutomi

Division of Materials Science and Chemical Engineering, Faculty of Engineering, Yokohama National University, Yokohama 240–8501, Japan

The delamination behavior of air plasma-sprayed thermal barrier coatings (APS-TBCs) exposed to heat in air at different temperatures was evaluated under mode II loading conditions. The TBC layer, BC layer, and substrate were composed of 8 mass% Y_2O_3 partially stabilized ZrO_2, NiCoCrAlY alloy, and Inconel 738 nickel base superalloy. The heat exposure was performed at 1173 K or 1423 K for 10 to 200 h. During the heat exposure, the thickness of thermally grown oxide (TGO) increased and the hardness of the bond coat (BC) layer near the TGO decreased with increasing heat exposure time. The delamination toughness decreased monotonically with increasing heat exposure time when the TBCs were heat exposed at 1173 K. In this case, delamination occurred at the TBC layer. The average thickness of the remaining TBC on the substrate side decreased with increasing exposure time. As for the TBCs exposed at 1423 K, the delamination toughness increased over the first 50 h, but then began to decrease with further exposure time. The delamination pathway has transferred to near the TGO layer. The fraction of TBC layer fracture decreased, whereas those of the TBC/TGO interface and TGO/BC interface fracture increased with increasing exposure time. The change in delamination toughness may have been caused by the interaction between the TGO thickening and the reduction of BC layer hardness. The increase in TGO thickness decreased the delamination toughness due to an increase in residual stresses. The decrease in hardness of the BC layer near the TGO may have increased the delamination toughness by increasing the plastic dissipation. [doi:10.2320/matertrans.M2016077]

(Received March 2, 2016; Accepted April 18, 2016; Published May 20, 2016)

Keywords: *air plasma-sprayed thermal barrier coatings, interfacial delamination toughness, mode II loading condition, plastic dissipation, pushout test*

1. Introduction

Thermal barrier coatings (TBCs) produced by an air plasma-spray (APS) process have been widely used as hot section components in gas turbines for thermal insulation and oxidation protection of nickel-base superalloy substrates. APS-TBCs are usually composed of an outer oxide ceramic TBC layer and an inner metallic bond coat (BC) layer to protect the substrate from high temperatures and oxidation[1–3]. Here, the TBC layer is also usually called as top coat (TC) layer. During service, the TBCs undergo thermal and/or thermo-mechanical loading. Sintering of the TBC layer[4,5], formation and growth of the thermally grown oxide (TGO) layer[2–8], and phase transformation of the BC layer[7–10] can occur during service. Microstructural changes in each layer and different loading conditions may influence the failure behavior of TBCs. It was reported that ultimate TBC failure might occur via an edge-and-buckle delamination mechanism[3]. A crack propagates along the TBC layer interface and/or interfaces under predominantly mode II loading conditions. Thus, it is important to understand the fracture properties of TBCs under shear loading conditions in order to evaluate their reliability.

Recently, conical indentation and wedge impression test methods that can evaluate delamination behavior under shear loading conditions have been developed[11–13]. Both methods can evaluate interfacial delamination by symmetrical crack propagation from the indented region. However, due to the low driving force for crack propagation and the difficulty of applying the unique vertical load to the coating, symmetrical crack propagation does not occur often. Barb[14–18], pushout[19–21], and other shear tests[22] have also been developed to measure delamination toughness under shear loading. Changes of delamination toughness in different interfacial roughness at as deposited state and in different heating condition such as isothermal heat exposure and thermal cycling have been evaluated in the electron beam physical vapor deposited TBCs (EB-PVD TBCs) by barb and pushout tests. Although the properties of the constituents and of the entire TBC system depend on the microstructure of the TBCs[4,7,8,23], the interfacial mechanical properties under mode II loading conditions in TBCs under different thermo-mechanical loading conditions that change the TBC microstructure are still not well understood. In this study, the microstructure development of APS-TBCs and changes in the delamination toughness under mode II loading conditions with different heat exposure temperatures and times were studied experimentally.

2. Experimental Procedure

2.1 Air plasma-sprayed thermal barrier coatings

TBCs were fabricated by a plasma spraying process. A thermal barrier coating layer consisting of 8 mass% Y_2O_3 partially stabilized ZrO_2 was coated on a bond coat (BC) layer by an air plasma-spraying process. The BC material was a NiCoCrAlY alloy (Co22 Cr17 Al12.5 Y0.6 and balance Ni in mass%) coated on a nickel base superalloy substrate (Inconel 738, Co8.5 Cr16 Al3.5 Ti3.5 W2.6 Mo1.8 Nb0.9 and balance Ni in mass%) by a low-pressure plasma-spraying process. The thicknesses of the TBC, BC, and substrate were ~250 μm, ~100 μm, and 3.2 mm, respectively. As-sprayed TBCs were heated in air at a heating rate of 1.6×10^{-1} K·s^{-1} to 1173 K or 1423 K and held there for 10, 50, 100, or 200 h. Then, the materials were cooled at 8.0×10^{-2} K·s^{-1} to room temperature.

[*1]Corresponding author, E-mail: hasegawa@ynu.ac.jp
[*2]Graduate Student, Yokohama National University. Present address: Ricoh Co., Ltd.

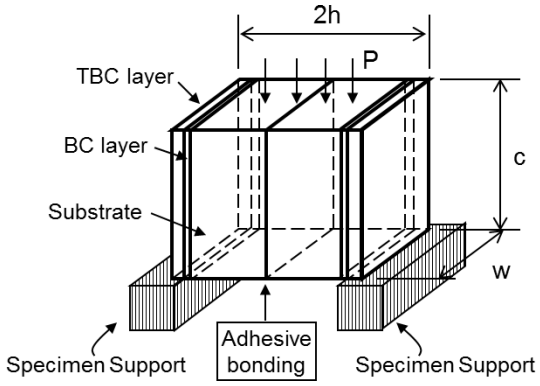

Fig. 1 Schematic illustration of the pushout test method.

Transverse sections of the TBCs after polishing to a 0.5 μm diamond paste finish were used for microstructure observations and analysis. Characterization of the microstructure was performed using an optical microscope (OM) and a scanning electron microscope (SEM). The Vickers hardness of the BC layer was measured in as-sprayed and heat exposed TBCs. A 0.49 N load was applied for 5 s and then removed.

2.2 Pushout test method

The pushout test method was used to measure the delamination behavior under shear loading conditions[19–21]. The substrate side of an APS-TBCs specimen was bonded using an epoxy-based adhesive and polished to form a pushout specimen. The surfaces of the pushout test specimens were carefully polished to a 0.5 μm diamond paste finish. Figure 1 shows a schematic configuration of the pushout test method. The specimens were 5 mm high (c), 4 mm wide (w), and 6.4 mm thick (2h). Tungsten carbide (WC) blocks were used for specimen support. The pushout tests were performed in air at room temperature using a screw-driven testing machine with a constant crosshead speed of 3.3 μm·s^{-1}. During the tests, the load and displacement were recorded by a data recorder with a sampling time of 0.1 s. After the pushout tests, the fracture surfaces of the specimens were observed from a side perpendicular to the loading axis (with an area of c × 2h in Fig. 1) of the specimen using OM and SEM.

3. Results and Discussion

3.1 Microstructural changes during heat exposure

Figure 2(a) shows a typical example of a polished transverse section of an as-sprayed APS-TBC. The TBC layer, BC layer, and substrate are visible. Pores and inter-splat boundaries were observed in the TBC layer as black spots and lines, respectively. Macroscopically, the BC layer seems to be a single phase. However, the high-magnification view shows that the BC layers are composed of a fine mixture of two phases, with bright and dark contrasts (Fig. 2(b)). These bright and dark contrasts are a γ' phase (Ni_3Al) with an L12-type structure and a β phase (NiAl) with a B2-type structure, respectively[8–10].

SEM micrographs of TGO and BC layers after heat exposure at 1173 K and 1423 K are shown in Fig. 3. The TBC layer was also observed near the BC layer. As for the specimens heat exposed at 1173 K, sintering of TBC layer should be occurred. However, the disappearance of pores and inter-splat boundaries suggests that sintering of the TBC layer could not be observed. In the specimen that was heat exposed at 1423 K, it is not so obvious but the fraction of pores and inter-splat boundaries seemed to decrease with increasing heat exposure time. This was due to sintering of the TBC layer during heat exposure. After 10 h of heat exposure at 1173 K (Fig. 3(a)), the BC layer separated into two different zones (hereafter expressed as Zone I and Zone II). Zone I was adjacent to the TBC layer and the substrate, was 6–7 μm thick, and consisted of a bright γ' phase. Zone II in between them consisted of a mixture of a bright γ' phase and a dark β phase. With increasing heat exposure time up to 50 h, the thicknesses of the zones next to the TBC layer (Zone Ia) and substrate (Zone Ib) both increase slightly. Almost all of the area in the BC layer (Zone II) was composed of a mixture of γ' and β phases (Fig. 3(b)–(d)). In the specimen heat exposed at 1423 K for 10 h (Fig. 3(e)), the BC layer also separated into two different zones (Zones I and II). With increasing heat exposure time, the thicknesses of Zones Ia and Ib increase, whereas that of Zone II decreases (Fig. 3(f)). Finally, Zone II completely disappears, and the entire BC layer becomes a γ' single phase (Fig. 3(g), (h)). The formation of a β depleted zone adjacent to the TBC layer (Zone Ia) and substrate (Zone Ib) is due to the consumption of Al by the formation and growth of the TGO layer and diffusion to the substrate, respectively[7,8]. Thus, the β phase transforms to the γ' phase.

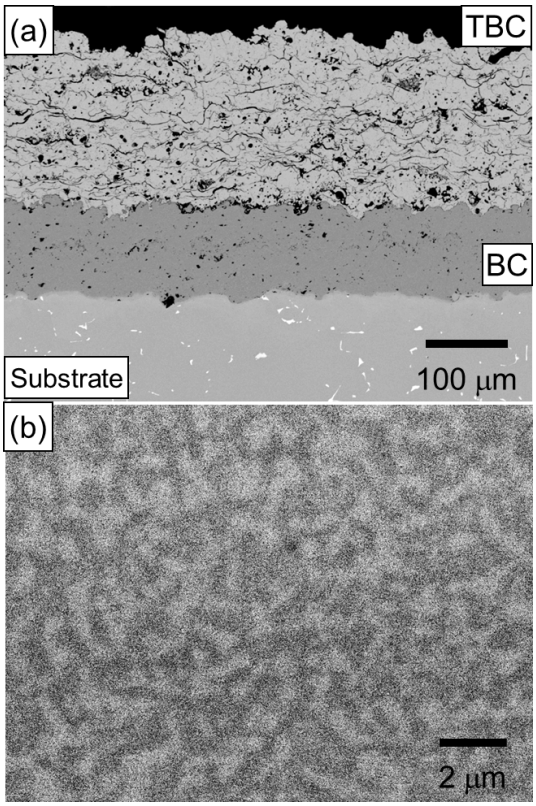

Fig. 2 Scanning electron micrographs of (a) as-sprayed thermal barrier coatings (TBCs) and (b) a high-magnification view of a bond coat (BC) layer.

The formation and growth of a continuous and irregularly shaped TGO layer was observed between the TBC and BC

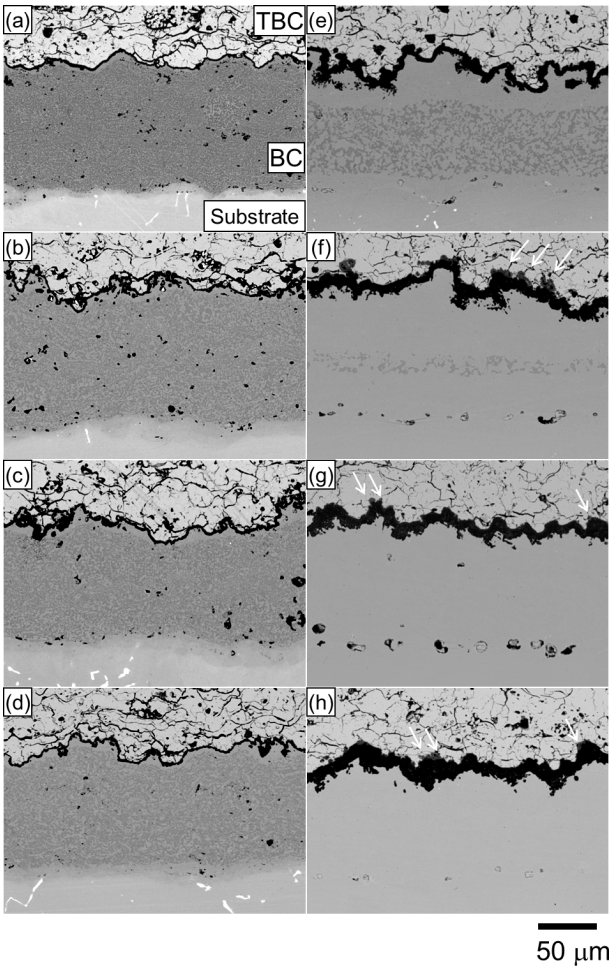

Fig. 3 Scanning electron micrographs of bond coat layer. The specimens were heat exposed at 1173 K for (a) 10, (b) 50, (c) 100, and (d) 200 h and at 1423 K for (e) 10, (f) 50, (g) 100, and (h) 200 h.

layers. Only a dark contrast region was observed in the TGO layer, indicating α-Al_2O_3 formation, when the specimens were heat exposed at 1173 K. When the specimens were heat exposed at 1423 K for more than 50 h, not only a dark contrast region but also a bright gray contrast region shown as white arrows in Fig. 3 indicating spinel with the composition of (Ni, Co)(Cr, Al)$_2$O$_4$ was observed[2,4,5]. Changes in the average thickness of the TGO layer $\bar{h}_{\mathrm{tgo}}$ with increasing heat exposure time t_h are plotted in Fig. 4. $\bar{h}_{\mathrm{tgo}}$ was measured by drawing 40 equally spaced lines at 7 μm intervals on an SEM photograph showing a polished transverse section of the coating. The lines were drawn normal to the BC/substrate interface. The thickness of the TGO layer increased with increasing heat exposure time. It has been reported that the thickness growth of the TGO layer can empirically be expressed as

$$\bar{h}_{\mathrm{tgo}} \approx k \cdot (t_h)^n \qquad (1)$$

where k and n are constants depending on the heat exposure conditions. In the present study, the values of n for specimens heat exposed at 1173 K and 1423 K were 0.37 and 0.32, respectively. These are nearly the same as the previously reported n values for APS-TBCs[5,6,24]. Another characteristic of TGO growth is increasing deviation of the TGO layer thickness with increasing heat exposure time. The reason for this phenomenon is believed to be the formation of spinel in a convex region[5,6].

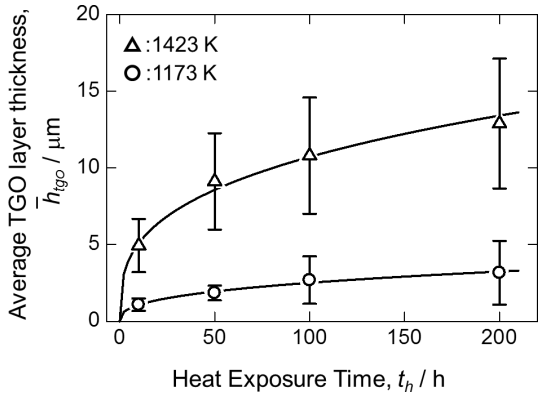

Fig. 4 Average TGO layer thickness after various heat exposure temperatures and times.

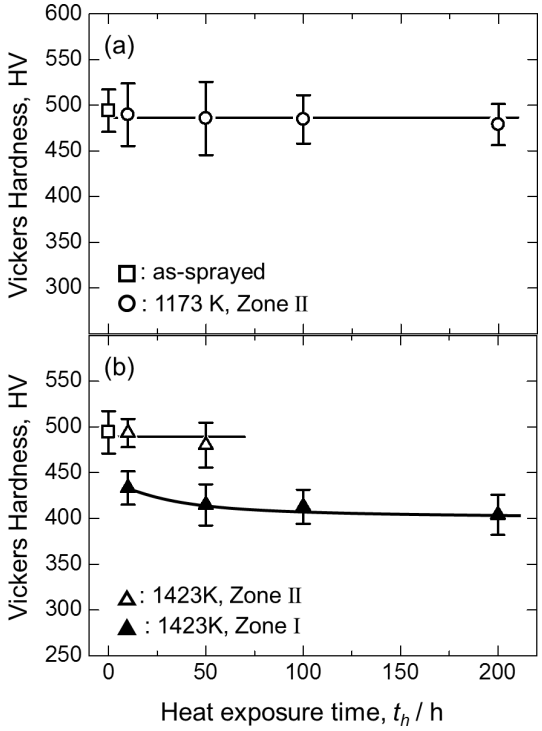

Fig. 5 Relationship between Vickers hardness of the BC layer and heat exposure time. Heat exposed at (a) 1173 K and (b) 1423 K.

Figure 5 shows the relationship between the Vickers hardness of the BC layer and the heat exposure time. The Vickers hardness was measured in the central regions of Zones I and II on the BC layer. The hardness of an as-sprayed BC layer is also plotted. In specimens heat exposed at 1173 K, the hardness of Zone I could not be measured due to its low thickness. In specimens heat exposed at 1423 K, the hardness of Zone I decreased with increasing heat exposure time (Fig. 5(b)). The hardness of Zone II, on the other hand, was independent of heat exposure temperature and time (Fig. 5 (a), (b)). Furthermore, the hardness of Zone II was higher than that of Zone I. Zones I and II consist of a γ' single-phase state and a (γ'+β) two-phase state, respectively. Thus, the observed difference in hardness may be because the β phase has a higher hardness than the γ' phase. Further, the change in hardness of Zone I in

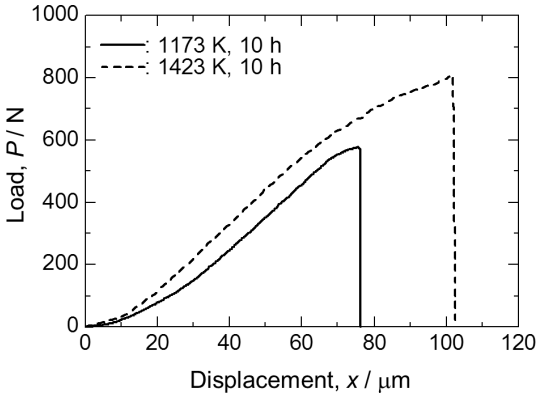

Fig. 6 Typical examples of load-displacement curves of pushout tests.

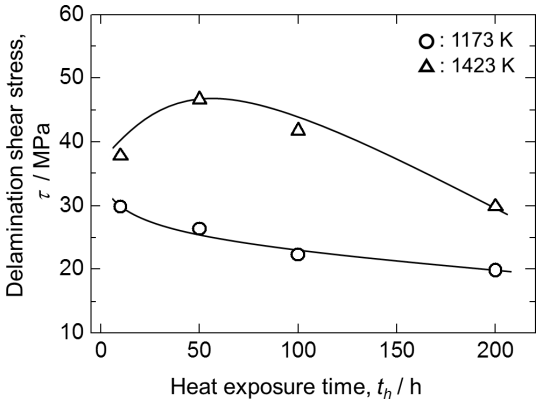

Fig. 7 Interfacial shear stress after different heat exposure temperatures and times.

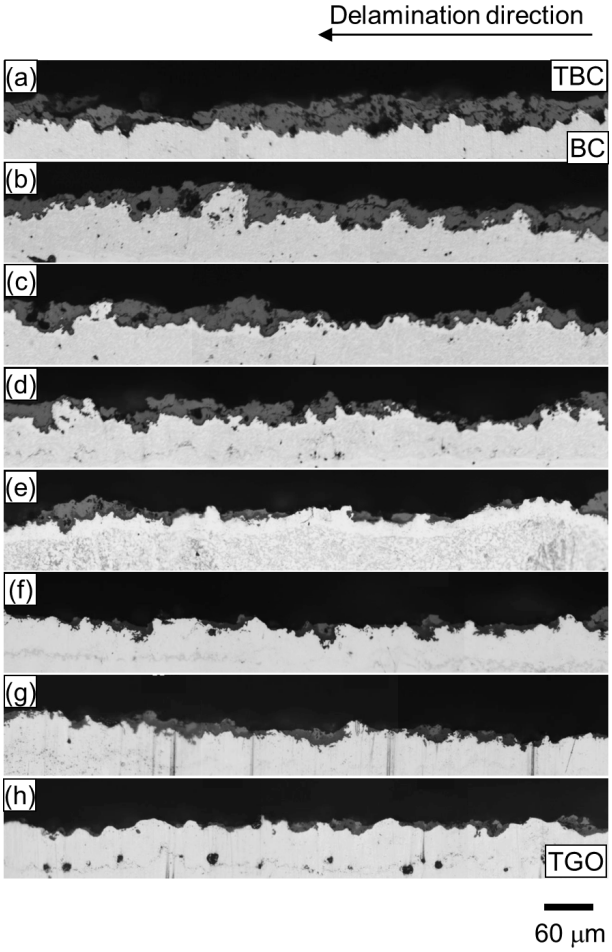

Fig. 8 Typical examples of delamination pathways. The specimens were heat exposed at 1173 K for (a) 10, (b) 50, (c) 100, and (d) 200 h and at 1423 K for (e) 10, (f) 50, (g) 100, and (h) 200 h.

specimens exposed at 1173 K may indicate almost the same hardness change in Zone I of the specimens exposed at 1473 K. This may be due to the same phase state in Zones I and II in each heat exposure condition and almost the same hardness at Zone II during the heat exposure at 1173 K and 1423 K.

3.2 Delamination under shear loading

A typical load-displacement curve for a pushout test is shown in Fig. 6. In this case, the specimens were heat exposed for 10 h at 1173 K and 1423 K. At the initial stage of loading in both specimens, a non-linear regime appeared due to a change in the compliance of the testing system. After this non-linear regime, the load increased almost linearly. Then, the slope of the curve decreased until the maximum load was reached. Finally, the load dropped to zero, indicating delamination of the coating. Figure 7 shows average delamination shear stress for different heat exposure times. Three specimens are tested in each heat exposure condition. Shear stresses in each condition are within the 20% of the average shear stress. In the specimen heat exposed at 1173 K, the delamination shear stress decreased with increasing heat exposure time. However, when the specimen was heat exposed at 1423 K, the delamination shear stress increased for 50 h of heat exposure and then decreased with further heat exposure time. Figure 8 shows typical examples of delaminated regions observed from the sides of the specimens in regions perpendicular to the loading direction (area of c × 2h in Fig. 1). Delamination was observed at the TBC layer in the specimen heat exposed at 1173 K (Fig. 8(a)–(d)). The average thickness of the remaining TBC layer at the substrate side, h_{tbc2}, was measured by drawing 50 equally spaced lines normal to the BC/substrate interface at 30 μm intervals on an OM photograph showing a polished transverse section of the coatings. The thickness of the remaining TBC layer was different for different positions. However, h_{tbc2} decreased with increasing heat exposure time. Furthermore, h_{tbc2} was 24.6, 20.7, 16.2, and 15.2 μm in specimens heat exposed at 1173 K for 10, 50, 100, and 200 h, respectively. In specimens heat exposed at 1423 K, the delamination pathway moved from the TBC layer to near the TGO layer. Delamination was observed in the TBC layer, TGO layer, or at the TBC/TGO and TGO/BC interfaces (Fig. 8(e)–(h)). It is difficult to define the fracture region in the case of delamination in the TGO layer and at the TBC/TGO interface. Thus, we hereafter express this as delamination at the TBC/TGO interface. h_{tbc2} decreased with increasing heat exposure time, and was 8.6, 7.7, 5.4, and 3.9 μm in specimens heat exposed at 1423 K for 10, 50, 100, and 200 h, respectively. The fraction of delaminated area as a function of heat exposure time at 1423 K is plotted in Fig. 9. The fraction of delaminated area was determined by measuring the length of the delaminated region parallel to the

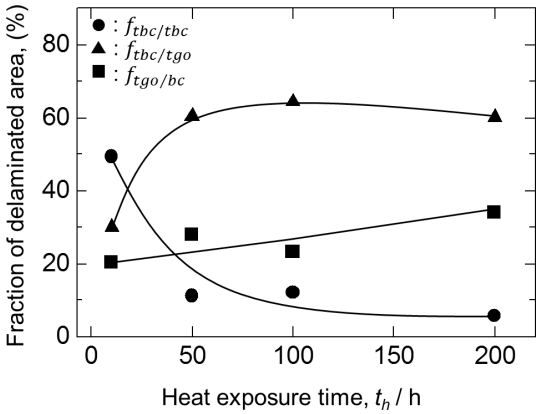

Fig. 9 Fraction of delaminated area as a function of heat exposure time at 1423 K.

BC/substrate interface on an OM photograph showing a polished transverse section of the coatings after a pushout test. The total length of the measured delaminated region in each specimen was approximately 3 mm. In a specimen heat exposed for 10 h, the fraction of TBC layer fracture $f_{\mathrm{tbc/tbc}}$ was approximately 50%. Further heat exposure decreased this fraction drastically, and it eventually fell below 10%. On the other hand, the fraction of TBC/TGO interface fracture $f_{\mathrm{tbc/tgo}}$ increased over the first 50 h of heat exposure but then became almost constant. The fraction of TGO/BC interface fracture $f_{\mathrm{tgo/bc}}$ increased linearly with increasing heat exposure time. Thus, the fracture paths in the present TBCs can be classified into three types, as schematically illustrated in Fig. 10. Stress conditions in each layer and substrate before and after the delamination are also shown in Fig. 10. In bonded area in each type, TBC and TGO layer shows compressive stress condition and substrate is showing tensile stress condition. As for the delaminated area in Type I, stress of delaminated TBC layer is almost zero. Remaining TBC layer and TGO layer are under compressive condition and substrate is in tensile condition. In case of Type II, stress in TBC layer is almost zero and TGO layer and substrate shows compressive and tensile stress condition, respectively. Regarding the delaminated area in Type III, TBC and TGO layer are under tensile and compressive stress condition and stress in substrate is almost zero. The main fracture path for the specimen heat exposed at 1173 K was Type I, and the TBC layer fractured by connecting the inter-splat boundary, regardless of the heat exposure time (Fig. 10(a)). In the specimen heat exposed at 1423 K, the main fracture pathway changed from the TBC layer (Type I) to the TBC/TGO interface (Type II, (Fig. 10(b))) and TGO/BC interface (Type III, (Fig. 10(c))) with increasing heat exposure time.

The transition of the fracture pathway from the TBC layer to near the TGO layer with increasing heat exposure time and thermal cycling time has been reported not only for Mode II loading conditions but also for Mode I and mixed mode loading conditions[7,25,26]. In wedge impression tests, which may apply Mode II loading to APS-TBCs, it has been reported that fracture occurs exclusively at the TBC layer in as-sprayed TBCs and TBCs with a TGO layer thickness below 5.5 μm. However, when the thickness is greater than 5.5 μm, the delamination pathway translates to the TGO layer[7]. In this

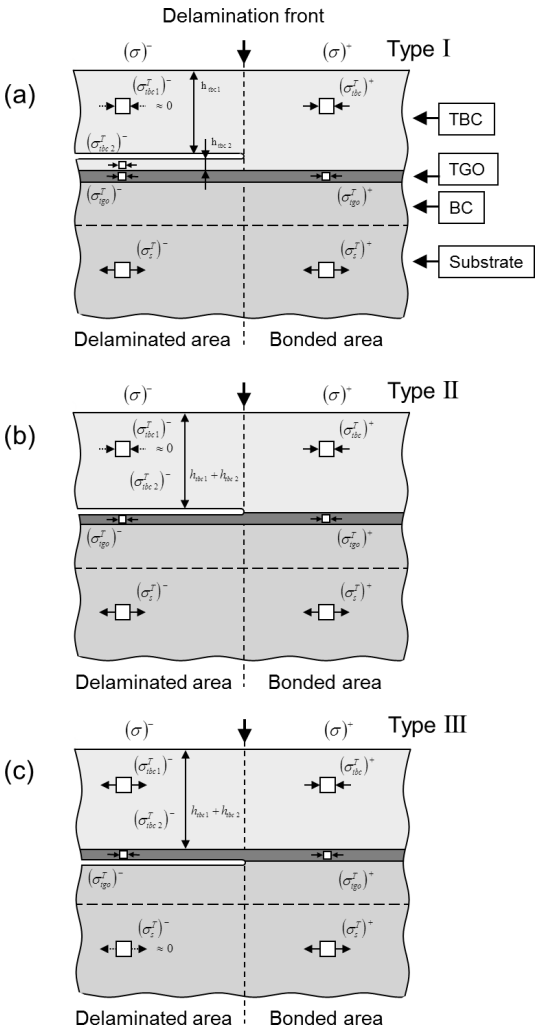

Fig. 10 Schematic illustration of three types of fracture path: (a) TBC layer (Type I), (b) TBC/TGO interface (Type II), and (c) TGO/BC interface (Type III).

study, nearly the same fracture behavior was observed. TBCs specimens heat exposed at 1173 K had an average TGO layer thickness of less than 5.5 μm, and fracture occurred within the TBC layer. Specimens heat exposed at 1423 K for more than 50 h had an average TGO layer thickness of more than 5.5 μm. In this case, the fracture mainly occurred near the TGO layer. In TBCs heat exposed at 1423 K for 10 h, the fracture occurred both within the TBC layer and near the TGO layer. This may be due to the scattering of the TGO layer thickness, as shown in Fig. 4, where the average thickness of the TGO layer was around 5 μm.

3.3 Delamination toughness

In order to measure the interfacial delamination toughness of TBCs using the pushout method, all of the constituent materials were assumed to undergo perfectly linear elastic deformation until coating delamination. Furthermore, it was assumed that all of the elastic strain energy stored within the specimen at maximum load was dissipated to form new delamination surfaces. The BC layer and the substrate were considered to be the same material because of the similarity of their chemical compositions. Based on these assumptions, the interfacial delamination toughness Γ_i can be given as[19,20],

Table 1 Material properties used for the calculation of delamination toughness.

Material	Young's modulus, E / GPa	Poisson's ratio, ν	Coefficient of thermal expansion, α / 10^{-6} K^{-1}	Thickness of Layer, h / μm
TBC	40	0.22	10.7	250
TGO	360	0.22	8	1.09–12.9
Substrate	197	0.3	16	3000

$$\Gamma_i \approx \frac{(\sigma_{\mathrm{tbc1}})^2}{2E^*_{\mathrm{tbc}}}h_{\mathrm{tbc1}} + \frac{(\sigma_{\mathrm{tbc2}})^2}{2E^*_{\mathrm{tbc}}}h_{\mathrm{tbc2}} + \frac{(\sigma_{\mathrm{tgo}})^2}{2E^*_{\mathrm{tgo}}}h_{\mathrm{tgo}} + \frac{(\sigma_s)^2}{2E^*_s}h_s + \Gamma_b \tag{2}$$

where σ and h are the in-plane stress parallel to the interface and the thickness of each layer and the substrate, respectively. Furthermore, $E^* = E/(1-\nu^2)$ is for plane strain and $E^* = E$ is for plane stress conditions. E and ν are Young's modulus and Poisson's ratio, respectively. The subscripts "tbc1", "tbc2", "tgo", and "s" indicate the delaminated TBC (TBC1) layer, remaining TBC (TBC2) layer, TGO layer, and substrate, respectively. Γ_b is the delamination toughness derived from the bending moment. Generally, the delamination toughness of interface crack between film and substrate under general edge loading condition will be calculated by the load parallel to the interface and the bending moment which will bend the film[27]. However, in case of the configuration of the pushout test, contribution of the bending moment to delamination toughness is low and could be assume as $\Gamma_b \approx 0$[19]. The in-plane stress of each layer is given as a summation of the thermal stress and maximum applied load of the layer, or,

$$\sigma_{\mathrm{tbc1}} = \sigma^T_{\mathrm{tbc1}} + \sigma^{\max}_{\mathrm{tbc1}} \tag{3}$$

$$\sigma_{\mathrm{tbc2}} = \sigma^T_{\mathrm{tbc2}} + \sigma^{\max}_{\mathrm{tbc2}} \tag{4}$$

$$\sigma_{\mathrm{tgo}} = \sigma^T_{\mathrm{tgo}} + \sigma^{\max}_{\mathrm{tgo}} \tag{5}$$

$$\sigma_s = \sigma^T_s + \sigma^{\max}_s. \tag{6}$$

The superscripts "T" and "max" indicate the thermal stress and maximum applied stress from the maximum applied load in the pushout test, respectively. The in-plane thermal stress of the TBC1 layer, TBC2 layer, TGO layer, and substrate and the maximum applied load at which the TBC layer, TBC/TGO interface, and TGO/BC interface fractured are described in the Appendix. The material properties used to calculate the interfacial delamination toughness are shown in Table 1[28]. Here, we assumed that the Young's modulus of TBC layer is almost constant and may not change sharply during heat exposure. It is reported that the significant increase of Young's modulus of TBC layer could be seen at temperatures above 1473 K[29]. However, when it was heated below 1373 K, it seems that the range of Young's modulus in the TBC layer is small. For the specimen heat exposed at 1173 K, fracture occurred at the TBC layer ($f_{\mathrm{tbc/tbc}} = 100\%$). In the specimen heat exposed at 1423 K, the fracture path changes as shown in Fig. 9. Thus, Γ, the delamination toughness of the heat exposed TBCs, is given as,

$$\Gamma = f_{\mathrm{tbc/tbc}} \cdot \Gamma_i^{\mathrm{tbc1/tbc2}} + f_{\mathrm{tbc/tgo}} \cdot \Gamma_i^{\mathrm{tbc/tgo}} + f_{\mathrm{tgo/bc}} \cdot \Gamma_i^{\mathrm{tgo/bc}} \tag{7}$$

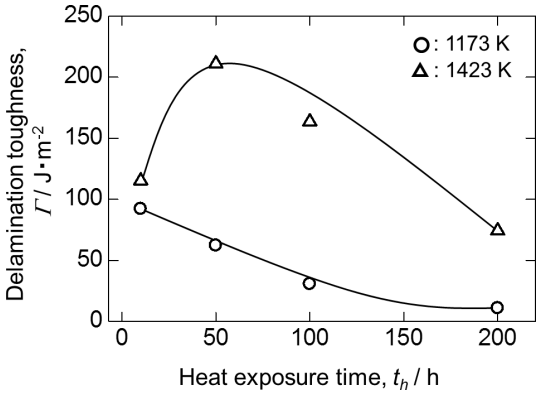

Fig. 11 Delamination toughness for various heat exposure temperatures and times.

where $\Gamma_i^{\mathrm{tbc1/tbc2}}$, $\Gamma_i^{\mathrm{tbc/tgo}}$, and $\Gamma_i^{\mathrm{tgo/bc}}$ are the interfacial delamination toughness for fracture at the TBC layer, TBC/TGO interface, and TGO/BC interface, respectively.

Figure 11 shows the change in delamination toughness after different heat exposure times at 1173 K and 1423 K. It can be seen that most of the specimens that were heat exposed at 1173 K had a lower toughness than specimens that were heat exposed at 1423 K. When the specimens were heat exposed at 1173 K for 10 h, the delamination toughness indicated the maximum value of ~92 $J{\cdot}m^{-2}$. With the increase in heat exposure time, the toughness decreased to ~11 $J{\cdot}m^{-2}$ after 200 h of heat exposure. Specimens heat exposed at 1423 K for 10 h had a toughness of ~115 $J{\cdot}m^{-2}$. 50 h of exposure increased the toughness to ~211 $J{\cdot}m^{-2}$. Increasing the exposure time further decreased the toughness to ~74 $J{\cdot}m^{-2}$ after 200 h of heat exposure. A similar increase and then decrease of toughness with increasing exposure time was also reported for EB-PVD TBCs under mode II loading conditions[19].

As shown in Fig. 8, the fracture of the TBC specimen that was heat exposed at 1173 K occurred within the TBC layer. With increasing exposure time, the thickness of the TGO layer increased (Fig. 4) and the thickness of the remaining TBC layer decreased. Thus, the decrease in delamination toughness with increasing exposure time may be due to an increase of the residual stress in the TBCs by the formation and growth of the TGO layer. In the specimen heat exposed at 1423 K for 10 h, the fraction of fracture in the TBC layer was approximately 50%. However, further heat exposure may cause the fracture path to move closer to the TGO layer. Thus, the decrease in toughness after 50 h of heat exposure may also be due to the increase in the residual stress of the TBCs because of the TGO growth.

On the other hand, the delamination toughness increased with increasing heat exposure time when the specimens were heat exposed for up to 50 h at 1423 K. Increasing TBC toughness with increasing aging time was also reported in four-point bending experiments under mixed mode loading conditions[26]. This increase was attributed to sintering of the TBC layer, as the fracture path was mainly within the TBC layer. In our research, the sintering of the TBC layer during heat exposure at 1423 K was also observed. However, in the fracture of the specimen heat exposed at 50 h, the main fracture pathway was near the TGO layer and the fraction of TBC layer fracture

was only 11%. Due to this difference in the main fracture path, the sintering of the TBC layer is unlikely to be the main reason for the increase in fracture toughness in this experiment. Recently, the delamination toughness of APS-TBCs that were heat treated in a vacuum at 1413 K was measured under mode II loading conditions[21]. Increasing delamination toughness and decreasing BC layer hardness were reported with increasing heat treatment time. Furthermore, the hardness of Zone I in the BC layer of a 50 h heat exposed specimen was lower than that of a 10 h heat exposed specimen. Therefore, the effects of plastic dissipation due to plastic deformation at the plastic zone of the BC layer may increase the delamination toughness with increasing heat exposure time up to 50 h. However, there is no evidence that plastic deformation actually occurs at BC layer when a crack propagates in the TBC layer or at the TBC/TGO interface near the BC layer. Further research is required for a more detailed understanding of this phenomenon.

4. Conclusions

The effects of heat exposure temperature on the mechanical and delamination properties of air plasma-sprayed thermal barrier coatings (APS-TBCs) were studied experimentally. The Vickers hardness of the BC layer adjacent to the TBC layer and the substrate (Zone I) decreased with increasing heat exposure time. In Zone II, which existed in between Zone I, the Vickers hardness was independent of heat exposure temperature and time. The hardness of Zone II was higher than that of Zone I. This was because the β phase was harder than the γ' phase. The fracture pathways in APS-TBCs can be classified into three types: TBC layer (Type I), TBC/TGO interface (Type II), and TGO/BC interface (Type III). The main fracture path for specimens heat exposed at 1173 K was within the TBC layer (Type I). The average thickness of the remaining TBC layer decreased with increasing heat exposure time. In specimens heat exposed at 1423 K, the main fracture pathway moved from the TBC layer (Type I) to the TBC/TGO interface (Type II) and TGO/BC interface (Type III) with increasing heat exposure time. Most of the specimens heat exposed at 1173 K had a lower delamination toughness than specimens heat exposed at 1423 K. The delamination toughness decreased monotonically with increasing heat exposure time when the TBCs were heat exposed at 1173 K. The delamination toughness increased during the first 50 h of heat exposure at 1423 K, but decreased with additional heat exposure time. The decrease in toughness at both heat exposure temperatures might be due to an increase in the residual stress of the TBCs caused by the formation and growth of the TGO layer. The increase in toughness was probably an effect of plastic dissipation due to the decreased hardness of the BC layer.

Acknowledgements

The authors would like to express their thanks to undergraduate student Mr. S. Ishii for his help in conducting experiments. This research was partially supported by grant-in-aid for young scientists (B) (23760662) from the Japan Society for the Promotion of Science. The authors greatly appreciate the grant.

REFERENCES

1) S.M. Meier and D.K. Gupta: Trans. AIME J. Eng. Gas Turbines Power **116** (1994) 250–257.
2) N.P. Padture, M. Gell and E.H. Jordan: Science **296** (2002) 280–284.
3) A.G. Evans, D.R. Mumm, J.W. Hutchinson, G.H. Meier and F.S. Pettit: Prog. Mater. Sci. **46** (2001) 505–553.
4) S. Guo and Y. Kagawa: Scr. Mater. **50** (2004) 1401–1406.
5) A. Shinmi, M. Hasegawa, Y. Kagawa, M. Kawamura and T. Suemitsu: J. Japan Inst. Metals **69** (2005) 67–72.
6) M. Tanaka, M. Hasegawa and Y. Kagawa: Mater. Trans. **47** (2006) 2512–2517.
7) A. Rabiei and A.G. Evans: Acta Mater. **48** (2000) 3963–3976.
8) M. Hasegawa and Y. Kagawa: Inter. J. Appl. Ceram. Technol. **3** (2006) 293–301.
9) C. Mennicke, D.R. Mumm and D.R. Clarke: Z. Metallk. **90** (1999) 1079–1084.
10) T. Rehfeldt, G. Schumacher, R. Vaßen, and R.P. Wahi: Scripta. Mater. **43** (2000) 963–968.
11) A. Vasinonta and J.L. Beuth: Eng. Fract. Mech. **68** (2001) 843–860.
12) D.R. Mumm and A.G. Evans: Acta Mater. **48** (2000) 1815–1827.
13) M.R. Begley, D.R. Mumm and A.G. Evans: Acta Mater. **48** (2000) 3211–3220.
14) S. Guo, D.R. Mumm, A.M. Karlsson and Y. Kagawa: Scr. Mater. **53** (2005) 1043–1048.
15) S. Guo, Y. Tanaka and Y. Kagawa: J. Eur. Cera. Soc. **27** (2007) 3425–3431.
16) Y.F. Liu, Y. Kagawa and A.G. Evans: Acta Mater. **56** (2008) 43–49.
17) N.Y. Cao, Y.F. Liu and Y. Kagawa: Surf. Coat. Tech. **202** (2008) 3109–3114.
18) N.Y. Cao, Y. Kagawa and Y.F. Liu: Surf. Coat. Tech. **202** (2008) 3413–3418.
19) S.S. Kim, Y.F. Liu and Y. Kagawa: Acta Mater. **55** (2007) 3771–3781.
20) M. Tanaka, Y.F. Liu, S.S. Kim and Y. Kagawa: J. Mater. Res. **23** (2008) 2382–2392.
21) M. Hasegawa, T. Endo and H. Fukutomi: J. Japan Inst. Metals **73** (2009) 802–808.
22) Z.-H. Xu, Y. Yang, P. Huang and X. Li: Acta Mater. **58** (2010) 5972–5979.
23) M. Tanaka, M. Hasegawa, A.F. Dericioglu and Y. Kagawa: Mater. Sci. Eng. A **419** (2006) 262–268.
24) U. Schulz, M. Menzebach, C. Leyens and Y.Q. Yang: Surf. Coat. Tech. **146–147** (2001) 117–123.
25) L.L. Shaw, B. Barber, E.H. Jordan and M. Gell: Scr. Mater. **39** (1998) 1427–1434.
26) Y. Yamazaki, A. Schmid and A. Scholz: Surf. Coat. Tech. **201** (2006) 744–754.
27) Z. Suo and J.W. Hutchinson: Int. J. Fract. **43** (1990) 1–18.
28) R. Vaßen, G. Kerkhoff and D. Stöver: Mater. Sci. Eng. A **303** (2001) 100–109.
29) J.A. Thompson and T.W. Clyne: Acta Mater. **49** (2001) 1565–1575.

Appendix

The interfacial delamination toughness Γ_i of TBCs was assumed to satisfy small scale yielding. Thus, the interfacial delamination toughness can be calculated as a balance between the stored strain energy per unit area of the TBCs in the bonded area and that in the delaminated area (Fig. 10). The stored strain energy per unit area of the TBCs is given by the thermal stress and maximum applied stress of the TBC layer, TGO layer, and substrate. Furthermore, the thermal stresses of the TBC layer, TGO layer, and substrate are assumed to derive from the thermal expansion mismatch between the layers. Here, the thermal stresses and maximum applied stresses in each layer and substrate in the bonded and delaminated

areas are given for various situations described below as cases A1 to A4.

A1 In-plane thermal stress along the interface of each layer and substrate on fully bonded TBCs

The in-plane thermal stresses of the TBC layer, TGO layer, and substrate on a fully bonded TBC are given by

$$(\sigma_{\mathrm{tbc1}}^{T})^{+} = -\frac{E_{\mathrm{tbc1}}^{*}\Delta T[E_{\mathrm{tbc2}}^{*}h_{\mathrm{tbc2}}(\alpha_{\mathrm{tbc1}}^{*}-\alpha_{\mathrm{tbc2}}^{*}) + E_{\mathrm{tgo}}^{*}h_{\mathrm{tgo}}(\alpha_{\mathrm{tbc1}}^{*}-\alpha_{\mathrm{tgo}}^{*}) + E_{s}^{*}h_{s}(\alpha_{\mathrm{tbc1}}^{*}-\alpha_{s}^{*})]}{E_{\mathrm{tbc1}}^{*}h_{\mathrm{tbc1}} + E_{\mathrm{tbc2}}^{*}h_{\mathrm{tbc2}} + E_{\mathrm{tgo}}^{*}h_{\mathrm{tgo}} + E_{s}^{*}h_{s}} \tag{A1-1}$$

$$(\sigma_{\mathrm{tbc2}}^{T})^{+} = \frac{E_{\mathrm{tbc2}}^{*}\Delta T[E_{\mathrm{tbc1}}^{*}h_{\mathrm{tbc1}}(\alpha_{\mathrm{tbc1}}^{*}-\alpha_{\mathrm{tbc2}}^{*}) + E_{\mathrm{tgo}}^{*}h_{\mathrm{tgo}}(\alpha_{\mathrm{tgo}}^{*}-\alpha_{\mathrm{tbc2}}^{*}) + E_{s}^{*}h_{s}(\alpha_{s}^{*}-\alpha_{\mathrm{tbc2}}^{*})]}{E_{\mathrm{tbc1}}^{*}h_{\mathrm{tbc1}} + E_{\mathrm{tbc2}}^{*}h_{\mathrm{tbc2}} + E_{\mathrm{tgo}}^{*}h_{\mathrm{tgo}} + E_{s}^{*}h_{s}} \tag{A1-2}$$

$$(\sigma_{\mathrm{tgo}}^{T})^{+} = \frac{E_{\mathrm{tgo}}^{*}\Delta T[E_{\mathrm{tbc1}}^{*}h_{\mathrm{tbc1}}(\alpha_{\mathrm{tbc1}}^{*}-\alpha_{\mathrm{tgo}}^{*}) + E_{\mathrm{tbc2}}^{*}h_{\mathrm{tbc2}}(\alpha_{\mathrm{tbc2}}^{*}-\alpha_{\mathrm{tgo}}^{*}) + E_{s}^{*}h_{s}(\alpha_{s}^{*}-\alpha_{\mathrm{tgo}}^{*})]}{E_{\mathrm{tbc1}}^{*}h_{\mathrm{tbc1}} + E_{\mathrm{tbc2}}^{*}h_{\mathrm{tbc2}} + E_{\mathrm{tgo}}^{*}h_{\mathrm{tgo}} + E_{s}^{*}h_{s}} \tag{A1-3}$$

$$(\sigma_{s}^{T})^{+} = \frac{E_{s}^{*}\Delta T[E_{\mathrm{tbc1}}^{*}h_{\mathrm{tbc1}}(\alpha_{\mathrm{tbc1}}^{*}-\alpha_{s}^{*}) + E_{\mathrm{tbc2}}^{*}h_{\mathrm{tbc2}}(\alpha_{\mathrm{tbc2}}^{*}-\alpha_{s}^{*}) + E_{\mathrm{tgo}}^{*}h_{\mathrm{tgo}}(\alpha_{\mathrm{tgo}}^{*}-\alpha_{s}^{*})]}{E_{\mathrm{tbc1}}^{*}h_{\mathrm{tbc1}} + E_{\mathrm{tbc2}}^{*}h_{\mathrm{tbc2}} + E_{\mathrm{tgo}}^{*}h_{\mathrm{tgo}} + E_{s}^{*}h_{s}} \tag{A1-4}$$

where $(\sigma_{\mathrm{tbc1}}^{T})^{+}$, $(\sigma_{\mathrm{tbc2}}^{T})^{+}$, $(\sigma_{\mathrm{tgo}}^{T})^{+}$, and $(\sigma_{s}^{T})^{+}$ indicate thermal stresses in the TBC layer, TGO layer, and substrate. $E^{*} = E/(1-\nu^{2})$ and $\alpha^{*} = 1+\alpha$ for plane strain and $E^{*} = E$ and $\alpha^{*} = \alpha$ for plane stress. E and α are the Young's modulus and the thermal expansion coefficient, respectively. Subscripts "tbc1", "tbc2", "tgo", and "s" refer to the TBC1 layer, TBC2 layer, TGO layer, and substrate, respectively. These values are assumed to be independent of temperature. ΔT is the temperature difference, which was assumed to be −400 K.

A2 In-plane thermal stress along the interface of each layer and substrate after delamination of the TBC layer and the maximum applied stress in the TBC layer, TGO layer, and substrate

The in-plane thermal stresses of the TBC layer, TGO layer, and substrate after delamination within the TBC layer on the TBCs are given by

$$(\sigma_{\mathrm{tbc1}}^{T})^{-} = 0 \tag{A2-1}$$

$$(\sigma_{\mathrm{tbc2}}^{T})^{-} = -\frac{E_{\mathrm{tbc2}}^{*}\Delta T[E_{\mathrm{tgo}}^{*}h_{\mathrm{tgo}}(\alpha_{\mathrm{tbc2}}^{*}-\alpha_{\mathrm{tgo}}^{*}) + E_{s}^{*}h_{s}(\alpha_{\mathrm{tbc2}}^{*}-\alpha_{\mathrm{tgo}}^{*})]}{E_{\mathrm{tbc2}}^{*}h_{\mathrm{tbc2}} + E_{\mathrm{tgo}}^{*}h_{\mathrm{tgo}} + E_{s}^{*}h_{s}} \tag{A2-2}$$

$$(\sigma_{\mathrm{tgo}}^{T})^{-} = \frac{E_{\mathrm{tgo}}^{*}\Delta T[E_{\mathrm{tbc2}}^{*}h_{\mathrm{tbc2}}(\alpha_{\mathrm{tbc2}}^{*}-\alpha_{\mathrm{tgo}}^{*}) + E_{s}^{*}h_{s}(\alpha_{s}^{*}-\alpha_{\mathrm{tgo}}^{*})]}{E_{\mathrm{tbc2}}^{*}h_{\mathrm{tbc2}} + E_{\mathrm{tgo}}^{*}h_{\mathrm{tgo}} + E_{s}^{*}h_{s}} \tag{A2-3}$$

$$(\sigma_{s}^{T})^{-} = \frac{E_{s}^{*}\Delta T[E_{\mathrm{tbc2}}^{*}h_{\mathrm{tbc2}}(\alpha_{\mathrm{tbc2}}^{*}-\alpha_{s}^{*}) + E_{\mathrm{tgo}}^{*}h_{\mathrm{tgo}}(\alpha_{\mathrm{tgo}}^{*}-\alpha_{s}^{*})]}{E_{\mathrm{tbc2}}^{*}h_{\mathrm{tbc2}} + E_{\mathrm{tgo}}^{*}h_{\mathrm{tgo}} + E_{s}^{*}h_{s}}. \tag{A2-4}$$

The in-plane maximum applied stresses of the TBC layer, TGO layer, and substrate can be described as

$$\sigma_{\mathrm{tbc1}}^{\max} = \frac{E_{\mathrm{tbc2}}^{*}h_{\mathrm{tbc2}} + E_{\mathrm{tgo}}^{*}h_{\mathrm{tgo}} + E_{s}^{*}h_{s}}{h_{\mathrm{tbc1}}(E_{\mathrm{tbc1}}^{*}h_{\mathrm{tbc1}} + E_{\mathrm{tbc2}}^{*}h_{\mathrm{tbc2}} + E_{\mathrm{tgo}}^{*}h_{\mathrm{tgo}} + E_{s}^{*}h_{s})} \cdot \frac{P}{w} \tag{A2-5}$$

$$\sigma_{\mathrm{tbc2}}^{\max} = -\frac{E_{\mathrm{tbc2}}^{*}}{E_{\mathrm{tbc1}}^{*}h_{\mathrm{tbc1}} + E_{\mathrm{tbc2}}^{*}h_{\mathrm{tbc2}} + E_{\mathrm{tgo}}^{*}h_{\mathrm{tgo}} + E_{s}^{*}h_{s}} \cdot \frac{P}{w} \tag{A2-6}$$

$$\sigma_{\mathrm{tgo}}^{\max} = -\frac{E_{\mathrm{tgo}}^{*}}{E_{\mathrm{tbc1}}^{*}h_{\mathrm{tbc1}} + E_{\mathrm{tbc2}}^{*}h_{\mathrm{tbc2}} + E_{\mathrm{tgo}}^{*}h_{\mathrm{tgo}} + E_{s}^{*}h_{s}} \cdot \frac{P}{w} \tag{A2-7}$$

$$\sigma_{s}^{\max} = -\frac{E_{s}^{*}}{E_{\mathrm{tbc1}}^{*}h_{\mathrm{tbc1}} + E_{\mathrm{tbc2}}^{*}h_{\mathrm{tbc2}} + E_{\mathrm{tgo}}^{*}h_{\mathrm{tgo}} + E_{s}^{*}h_{s}} \cdot \frac{P}{w} \tag{A2-8}$$

where $\sigma_{\mathrm{tbc1}}^{\max}$, $\sigma_{\mathrm{tbc2}}^{\max}$, $\sigma_{\mathrm{tgo}}^{\max}$, and $\sigma_{s}^{\max}$ indicate the maximum applied stresses of the TBC layer, TGO layer, and substrate. P and w are the applied load and width of the pushout specimen, respectively (Fig. 1).

A3 In-plane thermal stress along the interface of each layer and substrate after delamination at the TBC/TGO interface and the maximum applied stress of the TBC layer, TGO layer, and substrate

The in-plane thermal stresses of the TBC layer, TGO layer, and substrate after delamination at the TBC/TGO interface on the TBCs are given by

$$(\sigma_{\mathrm{tbc1}}^{T})^{-} = 0 \tag{A3-1}$$

$$(\sigma_{\mathrm{tgo}}^{T})^{-} = \frac{E_{\mathrm{tgo}}^{*}\Delta T[E_{s}^{*}h_{s}(\alpha_{s}^{*}-\alpha_{\mathrm{tgo}}^{*})]}{E_{\mathrm{tgo}}^{*}h_{\mathrm{tgo}} + E_{s}^{*}h_{s}} \tag{A3-2}$$

$$(\sigma_{s}^{T})^{-} = \frac{E_{s}^{*}\Delta T[E_{\mathrm{tgo}}^{*}h_{\mathrm{tgo}}(\alpha_{\mathrm{tgo}}^{*}-\alpha_{s}^{*})]}{E_{\mathrm{tgo}}^{*}h_{\mathrm{tgo}} + E_{s}^{*}h_{s}}. \tag{A3-3}$$

The in-plane maximum applied stresses of the TBC layer, TGO layer, and substrate are given by

$$\sigma_{\mathrm{tbc}}^{\max} = \frac{E_{\mathrm{tgo}}^{*}h_{\mathrm{tgo}} + E_{s}^{*}h_{s}}{h_{\mathrm{tbc}}(E_{\mathrm{tbc}}^{*}h_{\mathrm{tbc}} + E_{\mathrm{tgo}}^{*}h_{\mathrm{tgo}} + E_{s}^{*}h_{s})} \cdot \frac{P}{w} \tag{A3-4}$$

$$\sigma_{\mathrm{tgo}}^{\max} = -\frac{E_{\mathrm{tgo}}^{*}}{E_{\mathrm{tbc}}^{*}h_{\mathrm{tbc}} + E_{\mathrm{tgo}}^{*}h_{\mathrm{tgo}} + E_{s}^{*}h_{s}} \cdot \frac{P}{w} \tag{A3-5}$$

$$\sigma_{s}^{\max} = -\frac{E_{s}^{*}}{E_{\mathrm{tbc}}^{*}h_{\mathrm{tbc}} + E_{\mathrm{tgo}}^{*}h_{\mathrm{tgo}} + E_{s}^{*}h_{s}} \cdot \frac{P}{w}. \tag{A3-6}$$

A4 In-plane thermal stress along the interface of each layer and substrate after delamination at the TGO/BC interface and the maximum applied stress of the TBC layer, TGO layer, and substrate

The in-plane thermal stresses of the TBC layer, TGO layer, and substrate after delamination at the TGO/BC interface on the TBCs are given by

$$(\sigma_{\mathrm{tbc}}^{T})^{-} = \frac{E_{\mathrm{tbc}}^{*}\Delta T[E_{\mathrm{tgo}}^{*}h_{\mathrm{tgo}}(\alpha_{\mathrm{tgo}}^{*}-\alpha_{\mathrm{tbc}}^{*})]}{E_{\mathrm{tbc}}^{*}h_{\mathrm{tbc}} + E_{\mathrm{tgo}}^{*}h_{\mathrm{tgo}}} \tag{A4-1}$$

$$(\sigma_{\mathrm{tgo}}^{T})^{-} = \frac{E_{\mathrm{tgo}}^{*}\Delta T[E_{\mathrm{tbc}}^{*}h_{\mathrm{tbc}}(\alpha_{\mathrm{tbc}}^{*} - \alpha_{\mathrm{tgo}}^{*})]}{E_{\mathrm{tbc}}^{*}h_{\mathrm{tbc}} + E_{\mathrm{tgo}}^{*}h_{\mathrm{tgo}}} \quad \text{(A4-2)}$$

$$(\sigma_{s}^{T})^{-} = 0. \quad \text{(A4-3)}$$

The in-plane maximum applied stresses of the TBC layer, TGO layer, and substrate can be described as

$$\sigma_{\mathrm{tbc}}^{\max} = \frac{E_{\mathrm{tbc}}^{*}E_{s}^{*}h_{s}}{(E_{\mathrm{tbc}}^{*}h_{\mathrm{tbc}} + E_{\mathrm{tgo}}^{*}h_{\mathrm{tgo}})(E_{\mathrm{tbc}}^{*}h_{\mathrm{tbc}} + E_{\mathrm{tgo}}^{*}h_{\mathrm{tgo}} + E_{s}^{*}h_{s})} \cdot \frac{P}{w} \quad \text{(A4-4)}$$

$$\sigma_{\mathrm{tgo}}^{\max} = \frac{E_{\mathrm{tgo}}^{*}E_{s}^{*}h_{s}}{(E_{\mathrm{tbc}}^{*}h_{\mathrm{tbc}} + E_{\mathrm{tgo}}^{*}h_{\mathrm{tgo}})(E_{\mathrm{tbc}}^{*}h_{\mathrm{tbc}} + E_{\mathrm{tgo}}^{*}h_{\mathrm{tgo}} + E_{s}^{*}h_{s})} \cdot \frac{P}{w} \quad \text{(A4-5)}$$

$$\sigma_{s}^{\max} = -\frac{E_{s}^{*}}{E_{\mathrm{tbc}}^{*}h_{\mathrm{tbc}} + E_{\mathrm{tgo}}^{*}h_{\mathrm{tgo}} + E_{s}^{*}h_{s}} \cdot \frac{P}{w}. \quad \text{(A4-6)}$$